Applied Materials Today 31 (2023) 101741

Contents lists available at ScienceDirect

Applied Materials Today

journal homepage: www.elsevier.com/locate/apmt

[BMI*m*][BARF] imidazolium salt solutions in alkyl carbonate solvents: Structure and interactions

Marianna Mamusa [a], David Chelazzi [a], Michele Baglioni [b], Sergio Murgia [c], Emiliano Fratini [a], David Rivillo [d], Piet W.N.M. van Leeuwen [d], Henri S. Schrekker [d,*], Piero Baglioni [a,*]

[a] Department of Chemistry "Ugo Schiff" and CSGI, University of Florence, Via della Lastruccia 3, Sesto Fiorentino, Florence 50019, Italy
[b] Department of Biotechnology, Chemistry and Pharmacy and CSGI, Via Aldo Moro 2, Siena 53100, Italy
[c] Department of Life and Environmental Sciences, University of Cagliari, via Ospedale 72, Cagliari I-09124, Italy
[d] Institute of Chemistry, Universidade Federal do Rio Grande do Sul, Av. Bento Gonçalves 9500, Porto Alegre, RS 91501-970, Brazil

ARTICLE INFO

Keywords:
Imidazolium salts
Alkyl carbonates
Ionic liquids
[BMI*m*][BARF]
Nanostructure

ABSTRACT

Solutions of weakly coordinating ionic liquids (ILs) in alkyl carbonates are gaining growing attention, as the latter are "green" solvents with high solvation power, but the phase behavior and structure of ILs in organic polar solvents are still poorly understood. Here, we study the interactions and nanoscale structure of 1-butyl-3-methylimidazolium tetrakis[3,5-*bis*(*trifluoromethyl*)*phenyl*]borate, [BMIm][BARF], in three symmetrical alkyl carbonate solvents with increasing alkyl chain-length. Electrical conductivity and nuclear magnetic resonance measurements showed that [BMIm][BARF] was mostly undissociated in these solvents, especially at lower IL concentration. Small angle X-ray scattering patterns evidenced the presence of rod-like nanostructures in the IL/solvent mixtures. At higher IL concentration, [BMIm][BARF] is increasingly more dissociated in solvents with lower dielectric constant, as confirmed by analysis of the solvents' carbonyl stretching band via Fourier transform infrared spectroscopy. This trend is opposite to that exhibited by BMIm ILs with less bulky counterions. The bulky $BARF^-$ is weakly coordinating and has no ability to give strong H-bonding, thus short-range anisotropic van der Waals forces are likely key in the interaction of the ion pairs. The slower self-diffusion of the ions in alkyl carbonates with lower dielectric constants might partially hinder close contact needed for self-assembly into local nano-sized structures. Overall, our results shed light on interactions and self-organization in imidazolium salt-alkyl carbonate mixtures, with potential impact in applicative fields spanning from batteries, catalysis and extraction, up to bio-applications (antimicrobial and bioengineering).

1. Introduction

Ionic liquids (ILs), a class of compounds composed exclusively of ions, have gained growing attention in the past decades thanks to several interesting properties, such as negligible vapor pressure, nonflammability, and the ideally infinite anion/cation combinations that earned them the definition of "designer solvents" [1,2]. This promoted their widespread use in a large number of applications: among others, analytical and extraction techniques [3], catalysis [4], nanoreactors for colloidal templates [5], preparation of functional gels [6], superparamagnetic fluids [7], and conducting polymer composites [8]. Among the most extensively investigated types of ILs are those based on the *N,N*-dialkyl-substituted imidazolium cation, for which an extensive body of fundamental studies exists [9]; common anions are small inorganic species such as simple halides, tetrafluoroborate, hexafluorophosphate, and bis(trifluoromethylsulfonyl)imide [10–13]. Recently, the focus has shifted towards anions that show lower tendency to coordinate the cation owing to their bulky structures [14]. This is of significance, for instance, in electrochemical applications where the use of weakly coordinating anions can increase battery current and provide higher stability [15]. The use of ILs as electrolytes for improved batteries has been evaluated for some time now [16,17], especially in systems based on polar organic solvents providing high conductivity, reduced viscosity, and a wide electrochemical window [18–22]. Among these, alkyl carbonates have been extensively used as solvents and co-solvents in electrochemical applications, thanks to their ability to solvate ions [18] and their environmentally-friendly profile as "green" solvents. [23]

Nevertheless, the importance of understanding the phase behavior

* Corresponding authors.
E-mail addresses: henri.schrekker@ufrgs.br (H.S. Schrekker), baglioni@csgi.unifi.it (P. Baglioni).

https://doi.org/10.1016/j.apmt.2023.101741
Received 16 September 2022; Received in revised form 21 December 2022; Accepted 19 January 2023

and nanoscale structure of IL solutions in organic polar solvents has only recently been addressed [18,22,24–27]. The molecular and supramolecular properties of these systems originate from a rich and complex ensemble of forces, including ionic, dipolar, hydrogen bonding, dispersive, and π-π interactions [18,28]. The study of mixtures of ILs and organic solvents is therefore not always straightforward and still poorly explored [29].

In particular, although the self-assembly of imidazolium ILs was studied before, these were mostly focused on strongly and weakly hydrogen bonding anions [30], where h-bonding is responsible for the buildup of supramolecular or polymeric structures [31,32]. For instance, imidazolium ILs with weakly hydrogen bonding anions are of interest due to their use as electrolytes in polar organic solvents for improved batteries. However, the behavior of ILs solutions where ions interactions are not driven by hydrogen bonding needs further investigation, especially when the solutions include alkyl carbonate solvents with great applicative potential. This motivated us to study the solution properties of the IL 1-butyl-3-methyl-imidazolium tetrakis[3,5-*bis*(*trifluoromethyl*)*phenyl*]borate, [BMIm][BARF] (see the molecular structure reported in Fig. 1), whose anion has no hydrogen bonding character [33,34], in three alkyl carbonate "green" solvents: dimethyl, diethyl, and dibutyl carbonate (DMC, DEC, and DBC; structures reported in Fig. 1). The $BARF^-$ anion presents a rather bulky structure with a tetrahedral geometry around the central boron atom; in addition, electronic charge is dispersed strongly, which hinders coordination bonds. Contrary to the IL containing the similar tetraphenylborate anion, in which the bulky trifluoromethyl substituents are absent, there is no evidence of hydrogen bonding between the BARF anion and the BMIm cation [33], suggesting that BARF can be classified as non-coordinating anion owing to a combination of steric and strong electronic effects.

In particular, we estimated the fraction of dissociated IL by comparing the molar conductivity values obtained by electric conductivity and nuclear magnetic resonance diffusion measurements, while the nanostructure and supramolecular features of the solutions were evaluated by means of small-angle X-ray scattering, as well as Fourier transform infrared spectroscopy, in an effort to rationalize the relationship between transport properties and the nanoscale structure of [BMIm][BARF] solutions in alkyl carbonate solvents.

2. Materials and methods

The IL 1-butyl-3-methyl-imidazolium tetrakis[3,5-*bis*(*trifluoromethyl*)*phenyl*]borate, abbreviated [BMIm][BARF], was prepared in 56% isolated yield according to the procedure described by Finden et al. [26]. ^{1}H NMR ($CDCl_3$) δ 7.78 (m, 1H), 7.68 (m, 8H), 7.53 (m, 4H), 7.02 (m, 1H), 6.93 (m, 1H), 3.94 (t, 2H, 3 J = 7.6 Hz), 3.65 (s, 3H), 1.74 (m, 2H), 1.24 (m, 2H), 0.91 (t, 3H, 3 J = 7.6 Hz). $C_{80}H_{54}B_2F_{48}N_4$, MW = 2004.89 g.mol^{-1}, M_p = 104 °C.

Dimethyl carbonate (DMC, ≥ 99%; MW = 90.08 g·mol^{-1}), diethyl carbonate (DEC, ≥ 99%; MW = 118.13 g·mol^{-1}) and dibutyl carbonate (DBC, ≥ 99%; MW = 174.24 g·mol^{-1}) were purchased from Sigma-Aldrich and used without further purification.

2.1. Samples preparation

Solutions of [BMIm][BARF] in DMC, DEC and DBC were prepared at concentrations of 5, 10, 30, 50 and 70% (wt%) for each solvent, in quantities 0.5 g for each solution in glass vials. The vials were sealed with parafilm and stored at 25 °C (± 0.5 °C) for the entire duration of the study. The samples were equilibrated for two weeks before measurements.

2.2. Electrical conductivity

The electrical conductivity (σ) of the [BMIm][BARF] solutions in alkyl carbonate solvents was measured at 25 °C using a S230 SevenCompact conductivity meter (Mettler-Toledo) with ± 0.5% accuracy, and a micro conductivity cell (InLab 751–4 mm, Mettler-Toledo) equipped with two platinum poles, a chemical resistant glass body, and integrated temperature probe. The cell constant was calibrated with a standard 0.01 M KCl solution.

2.3. Nuclear magnetic resonance (NMR)

A Bruker Avance 300 MHz (7.05 T) spectrometer with a ^{1}H operating frequency of 300.131 MHz was used to measure the IL alkyl carbonate solutions. The field gradients (up to 1.2 T m) necessary to measure the self-diffusion coefficients were generated by a Bruker DIFF30 probe supplied by a Bruker Great 1/40 amplifier. All the measurements were carried out at 25 °C, and the temperature was kept constant (with an accuracy of 0.5 °C) by means of a Bruker Variable Temperature unit (BVT 3000). The pulsed gradient stimulated echo (PGSTE) sequence was used. Self-diffusion coefficients were obtained by varying the gradient strength (g) while keeping the gradient pulse length (δ) and the gradient pulse intervals constant within each experimental run. The Stejskal−Tanner equation (Eq. (1)) was used to fit recorded data [35]:

$$\frac{I}{I_0} = \exp^{\left[-DQ^2(\Delta-\delta/3)\right]} \quad (1)$$

where I and I_0 are the NMR signal intensities in the presence or absence of the applied field gradient, $Q = \gamma g \delta$ is the scattering vector (γ is the gyromagnetic ratio of the observed nucleus), ($\Delta - \delta/3$) is the diffusion time, Δ is the delay time between the encoding/decoding gradients, and D is the self-diffusion coefficient to be calculated.

2.4. Small-angle X-ray scattering (SAXS)

SAXS experiments were performed on an S3micro X-ray system from Hecus GMBH (Graz), equipped with an ultra-brilliant point microfocus source Genix-Fox 3D (Xenocs, Grenoble). The impinging radiation was the 1.542 Å CuK-α, produced by a sealed-tube generator (Seifert ID-303) operating at 2 kW. The detectors (OED 50 M) contained 1024 channels

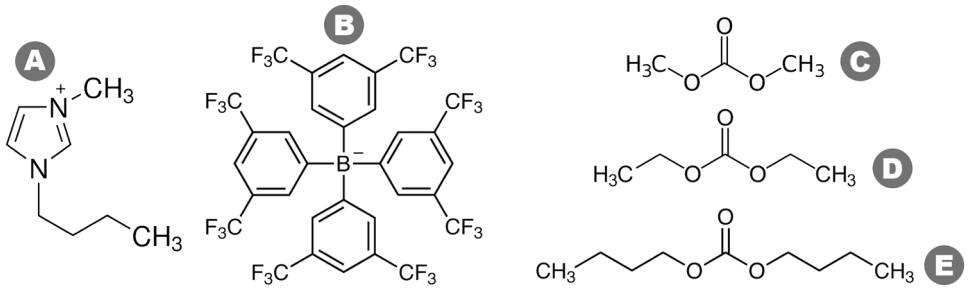

Fig. 1. Chemical structures of the IL, composed by (A) 1-butyl-3-methyl-imidazolium and (B) tetrakis[3,5-*bis*(*trifluoromethyl*)*phenyl*]borate [BMIm][BARF], together with the three alkyl carbonates: (C) dimethyl carbonate, (D) diethyl carbonate, and (E) dibutyl carbonate.

of 54 μm width, and the sample-to-detector distance was 280 mm. The primary beam was masked by a 2 mm W filter allowing for a *q*-range 0.009–0.54 $Å^{-1}$. Samples were placed either in quartz Mark capillaries (2 mm diameter) or paste sample holders. Measurements were performed under vacuum at 25.0 ± 0.1 °C (temperature controlled by a Peltier element). The resulting scattered intensity *I(q)* was plotted as a function of the scattering vector *q*, whose modulus is equal to $4\pi/\lambda \sin\theta$, with 2θ being the angle between the incident and scattered beams. Data reduction and modeling were carried out with Igor Pro (Wavemetrics, Inc.), using the analysis suite developed at the NIST Center for Neutron Research [36]. The X-ray scattering length densities of [BMIm][BARF] and the alkyl carbonate solvents (DMC, DEC, DBC) are listed in Table 1.

2.5. Attenuated total reflectance Fourier transform infrared spectroscopy (ATR-FTIR)

ATR-FTIR analysis was carried out on alkyl carbonates and their IL solutions using a ThermoNicolet Nexus 870 equipped with a Golden Gate diamond cell and a MCT detector (Mercury Cadmium Tellurium). The spectra were recorded between 650 and 4000 cm^{-1}, with a spectral resolution of 4 cm^{-1} and 128 scans for each spectrum. Each IL solution was analyzed in quadruplet, and the average spectrum calculated. The spectra of each series of IL solutions (in DBC, DEC and DMC) were normalized to the most intense CH stretching absorption of the corresponding alkyl carbonate (DBC: 2960 cm^{-1}; DEC: 2985 cm^{-1}; DMC: 2962 cm^{-1}).

3. Results and discussion

[BMI*m*][BARF] formed homogeneous mixtures with each of the three alkylcarbonate solvents at all tested concentrations up to 70%, appearing as macroscopically isotropic solutions with increasing viscosity. Instead, above 70%, a phase separation was observed at higher concentrations for all three solvents. It is worth mentioning that, in preliminary tests, similar mixtures of [BMIm][BARF] were also prepared in propylene carbonate (PC), the most common carbonate solvent used as battery electrolyte medium, and the same type of macroscopic phase behavior was observed as with DMC, DEC and DBC; however, the study of the PC solutions was not pursued further since they cannot be investigated by X-ray scattering, as [BMIm][BARF] and PC have almost identical X-ray scattering length density (SLD) values.

Most studies investigating mixtures of ILs with organic polar solvents [26,37] aim to evaluate their properties as possible battery electrolytes, with the organic solvents acting as media to increase conductivity by two distinct actions: i) reduction of the IL's viscosity, and ii) separation of the IL ion pair by solvation of the individual ions. With such purpose in mind, conductivity measurements of the [BMIm][BARF] stable solutions (5–70 wt%) in DMC, DEC, and DBC were performed. The values of electric conductivity (σ) followed the usual trend found in the literature, i.e., the conductivity increased initially with IL concentration in each solvent, and then decreased after reaching a maximum from 50% to 70% IL content (see Table 2) [26,37]. The σ values were in general in the order of 1–5 mS, evidencing poor transport properties in these systems. For a better understanding of this behavior, the calculated molar conductivities (Λ) were compared to those extrapolated from the NMR self-diffusion coefficients of the anion and the cation (Λ_{NMR}) using the Nerst-Einstein equation (Eq. (2)) [38]:

$$\Lambda_{NMR} = \frac{F^2}{RT}(D_+ + D_-) \quad (2)$$

where F is the Faraday constant, R is the gas constant, T is the temperature, and $D_\pm$ are the self-diffusion coefficients of the ions obtained by PGSTE NMR experiments (also given in Table 2).

Indeed, while the Λ values are the consequence of charged species migrating under the effect of an electric field, Λ_{NMR} values are obtained from Eq. (2) under the assumption that all the diffusing species observed in the NMR experiment, characterized by a unitary activity coefficient, contribute to the calculated molar conductivity. Since ions can exist in solution either as neutral aggregates or as ion pairs, this implicitly means that the Λ/Λ_{NMR} ratio gives the percentage of non-aggregated diffusing species (solvated ions) contributing to the measured conductivity. Such a piece of information may be helpful in clarifying the transport properties of the studied systems. The very low Λ/Λ_{NMR} ratios reported in Table 2 prove that only a small fraction of [BMIm][BARF] was in ionic form in all the investigated solutions. When DMC was used as solvent, dilution did not significantly affect the degree of ionization. Instead, when [BMIm][BARF] was dissolved in DEC or DBC the degree of ionization was further suppressed upon dilution, a phenomenon that seems to be correlated with the length of the alkyl chain of the solvent, or with its dielectric constant (DMC, DEC, and DBC possess the following dielectric constants: 3.2, 2.8, and 2.6; see Table 3) [39–41], and, in turn, to the nanostructures that are formed by [BMIm][BARF] in the three solvents, which were evidenced by the analysis of small X-ray scattering (SAXS) data. In addition, the percentage difference between D_+ and D_-, for each salt solution, increases from negligible (or close to the standard errors) at low salt concentration, up to ca. 25–40% in the most concentrated solutions. This might suggest the presence of ion aggregates at lower concentrations.

It should be also observed that, independently of the solvent used, the $D\pm$ values in Table 2 show a monotonic decrease for increasing [BMIm][BARF] concentration, without abrupt changes. This trend can be easily explained considering the increased viscosity of the solutions while increasing the salt content.

Scattering measurements were performed for a better characterization of the mixtures' structures at the nanoscale, completing the dynamic information obtained by conductivity measurements with the insights provided by a static technique such as SAXS. Scattering profiles collected for all the investigated samples are plotted in Fig. 2, together with their best fitting curves. The patterns show a common trend: a decreasing forward scattering intensity, *I(0)*, and a change in the shape of scattering with increasing IL content in each solvent. Recent SAXS investigations of IL/organic solvent mixtures have evidenced that the interpretation of such scattering patterns can be complicated by the coexisting nanostructures formed by pure phases of both compounds, generated by the different intermolecular forces at play (Coulombic, dipolar-dipolar, hydrogen bonding, van der Waals) [29], and that systems appearing completely miscible can reveal density and concentration fluctuations at the nanoscale [42].

Indeed, the shape of scattering curves, especially at lower IL concentration, suggested the existence of some nanostructured aggregates; moreover, since the slope of *I(q)* in the medium-*q* range was proportional to q^{-1}, the presence of rod-like particles in solution was considered. Several different models were tried to fit the data, but the best and more physically reliable results were obtained using a cylindrical model with a polydisperse radius. In the adopted model, the function calculated is the orientationally-averaged form factor of a cylinder of radius *R* and length *L*, which is then averaged according to a Schulz distribution of *R*. The mathematical expression for this form factor is then [43]:

$$P(q) = \frac{scale}{V_{poly}} \int_0^x f(r)dr \int_0^{\pi/2} F^2(q,\alpha)\sin\alpha d\alpha \quad (3)$$

Table 1
X-ray scattering length density (SLD, ρ) values for the compounds used in this work.

Compound	SLD, ρ ($Å^{-2}$)
[BMIm][BARF]	1.30×10^{-05}
DMC	9.61×10^{-06}
DEC	8.91×10^{-06}
DBC	8.59×10^{-06}

Table 2
Concentration (C), electric conductivity (σ) and corresponding molar conductivity (Λ = σ/C), diffusion coefficients for the cation (D_+) and the anion (D_-), and corresponding extrapolated molar conductivity (Λ_{NMR}), for all the solutions investigated in this paper. DMC = dimethyl carbonate; DEC = diethyl carbonate; DBC = dibutyl carbonate. Standard errors on the final Λ/Λ_{NMR} are in the order of 5%.

Solvent	[BMIm][BARF] wt%	C (mol/cm^3)	σ (S/cm)	Λ (S.cm^2/mol)	D_+ (cm^2/s)	D_- (cm^2/s)	Λ_{NMR} (S.cm^2/mol)	Λ/Λ_{NMR}
DMC	5	2.71×10^{-2}	6.40×10^{-4}	2.36×10^{-2}	4.70×10^{-10}	4.21×10^{-10}	3.35×10^{-1}	0.07
	10	5.50×10^{-2}	1.97×10^{-3}	3.58×10^{-2}	4.70×10^{-10}	4.14×10^{-10}	3.32×10^{-1}	0.11
	30	1.76×10^{-1}	5.50×10^{-3}	3.12×10^{-2}	3.85×10^{-10}	2.96×10^{-10}	2.56×10^{-1}	0.12
	50	3.15×10^{-1}	4.36×10^{-3}	1.39×10^{-2}	2.08×10^{-10}	1.43×10^{-10}	1.32×10^{-1}	0.11
	70	4.75×10^{-1}	1.66×10^{-3}	3.50×10^{-3}	6.75×10^{-11}	3.96×10^{-11}	4.02×10^{-2}	0.09
DEC	5	2.48×10^{-2}	3.15×10^{-4}	1.27×10^{-2}	3.78×10^{-10}	3.98×10^{-10}	2.92×10^{-1}	0.04
	10	5.05×10^{-2}	1.03×10^{-3}	2.04×10^{-2}	3.52×10^{-10}	3.03×10^{-10}	2.46×10^{-1}	0.08
	30	1.64×10^{-1}	3.53×10^{-3}	2.15×10^{-2}	2.64×10^{-10}	2.03×10^{-10}	1.75×10^{-1}	0.12
	50	2.98×10^{-1}	3.61×10^{-3}	1.21×10^{-2}	1.36×10^{-10}	9.72×10^{-11}	8.76×10^{-2}	0.14
	70	4.58×10^{-1}	1.63×10^{-3}	3.56×10^{-3}	3.76×10^{-11}	2.17×10^{-11}	2.23×10^{-2}	0.16
DBC	5	2.39×10^{-2}	6.70×10^{-4}	2.80×10^{-3}	1.37×10^{-10}	1.24×10^{-10}	9.81×10^{-2}	0.03
	10	4.87×10^{-2}	0.26×10^{-3}	5.29×10^{-3}	1.32×10^{-10}	1.19×10^{-10}	9.43×10^{-2}	0.06
	30	1.59×10^{-1}	1.15×10^{-3}	7.23×10^{-3}	9.71×10^{-11}	8.23×10^{-11}	6.74×10^{-2}	0.11
	50	2.91×10^{-1}	1.66×10^{-3}	5.69×10^{-3}	4.22×10^{-11}	3.15×10^{-11}	2.77×10^{-2}	0.21
	70	4.51×10^{-1}	0.57×10^{-3}	1.27×10^{-3}	1.35×10^{-11}	8.21×10^{-12}	8.16×10^{-3}	0.16

Table 3
Low-frequency dielectric constants at 298 K for the three alkyl carbonates ([a] from Ref. [39]; [b] from Ref. [40]; [c] from Ref. [41]). DBC = dibutyl carbonate; DEC = diethyl carbonate; DMC = dimethyl carbonate.

Solvent	Dielectric constant ε (at 298 K)
DMC	3.2 [a]
DEC	2.8 [b]
DBC	2.6 [c]

where *f(r)* is the normalized Schulz distribution of the radius. The limits of *f(r)* integration are adjusted automatically to cover the full range of radius (hence the *x* in the integral). The calculation is also normalized to the polydisperse volume, V_{poly}, using the second moment, as reported in Eq. (4):

$$V_{poly} = \pi r^2 L\left(\frac{z+2}{z+1}\right) \tag{4}$$

where *L* is, again, the cylinder length, and *z* is the width parameter of the Schulz distribution, described by Eq. (5):

$$z = \frac{1}{\left(\frac{\sigma}{\langle R\rangle}\right)^2} - 1 \tag{5}$$

being σ^2 the variance of the distribution. Finally, the scattering amplitude, *F(q,α)*, is given by Eq. (6):

$$F(q,\alpha) = 2V_{cyl}(\rho_{cyl} - \rho_{solv}) j_0(qH\cos\alpha)\frac{J_1(qr\sin\alpha)}{(qr\sin\alpha)} \tag{6}$$

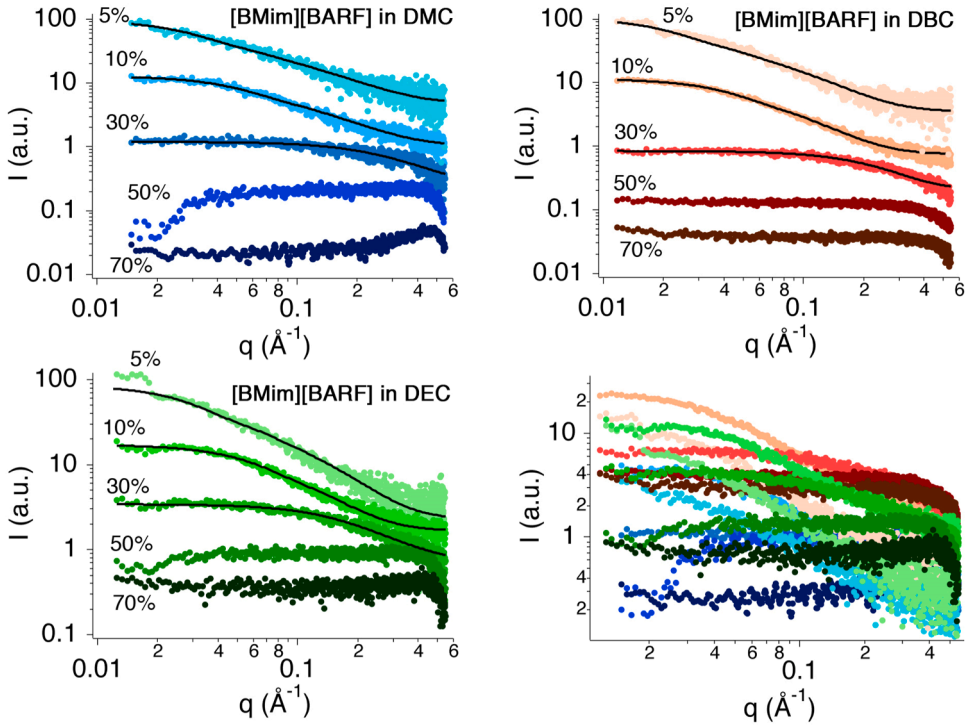

Fig. 2. SAXS patterns for [BMIm][BARF] in dimethyl carbonate (DMC), diethyl carbonate (DEC), and dibutyl carbonate (DBC). IL contents (wt%) are indicated next to each curve. The curves have been offset along the y axis to help readability. Best fittings are reported as solid black lines. The bottom-right graph shows all the scattering curves together without offsets, for sake of completeness.

where V_{cyl} is expressed by Eq. (7) as:

$$V_{cyl} = \pi R^2 L \tag{7}$$

and *j0(x)* is a sinusoidal function described by Eq. (8):

$$j_0(x) = \frac{\sin x}{x} \tag{8}$$

where *H=L/2, $J_1(x)$* is the first order Bessel function, and α is the angle between the cylinder axis and the scattering vector *q*. The second integral in Eq. (3), the one over α, averages all the form factors over all possible orientations of the cylinder with respect to *q*. In this model no interparticle interactions was taken into account, so that *I(q)* was finally obtained by multiplying the averaged *P(q)* by the volume fraction of the aggregates.

Only the scattering curves collected on 5–30% IL samples could be fitted using the aforementioned model. In fact, 50% and 70% scattering profiles are almost flat, indicating that the existing nanostructures at lower concentration are lost when IL/solvent ratio reaches the 1:1 threshold. Actually this critical concentration boundary is also well visible looking at molar conductivity data, which abruptly drop (especially in the case of [BMIm][BARF] in DMC and DEC) above 30% of IL.

Anyway, the trend emerging from the fitting data, reported in Table 4, is quite clear and coherent with what observed through conductivity and NMR measurements. Non-interacting rod-like IL aggregates were found in all three alkyl carbonate solvents, with a length inversely proportional to the dielectric constant of the solvent (for the 5% samples, 22 nm in DBC, and 16 nm in DEC and DMC). This is reasonable since the persistence length of such structures is higher in solvents with lower dielectric constant, where solvents are less capable of perturbing the [BMIm][BARF] aggregates. It is worth noting that the diameter of the rod-like aggregates is just 5–8 Å, which is consistent with the stacking of a single line of IL cations and anions to form elongated poly(ionic liquid) structures, surrounded by alkyl carbonate molecules, as schematized in Fig. 3. The very high values of radius polydispersity are in agreement with the hypothesized structure, since the "cylindrical" particle mathematically described by the fitting model has in fact a poorly defined geometrical interface. When IL concentration is increased to 10% and then 30% the same trend is observed for [BMIm][BARF] in all the three solvents, i.e., the length of the rod-like stacked poly-IL chains is significantly decreased, with slightly elongated structures that remain visible only in DBC when IL reaches 30%. For higher concentrations of [BMIm][BARF] aggregates or nanostructured inhomogeneities disappear.

Table 4
Main fitting results obtained from the analysis of 5–30% [BMIm][BARF] scattering profiles in the three alkyl carbonates. $Poly_R$ is the polydispersity of the radius R.

Solvent	[BMIb][BARF] concentration	Radius (nm)	Length (nm)	$Poly_R$
DMC	5%	0.22 ± 0.01	16 ± 1	0.7 ± 0.1
	10%	0.23 ± 0.01	9 ± 1	0.7 ± 0.1
	30%	0.26 ± 0.01	0.4 ± 0.1	0.7 ± 0.1
DEC	5%	0.28 ± 0.01	16 ± 1	0.7 ± 0.1
	10%	0.33 ± 0.01	8 ± 1	0.7 ± 0.1
	30%	0.40 ± 0.01	0.5 ± 0.1	0.7 ± 0.1
DBC	5%	0.27 ± 0.01	22 ± 1	0.8 ± 0.1
	10%	0.32 ± 0.01	11 ± 1	0.8 ± 0.1
	30%	0.38 ± 0.01	1.0 ± 0.1	0.6 ± 0.1

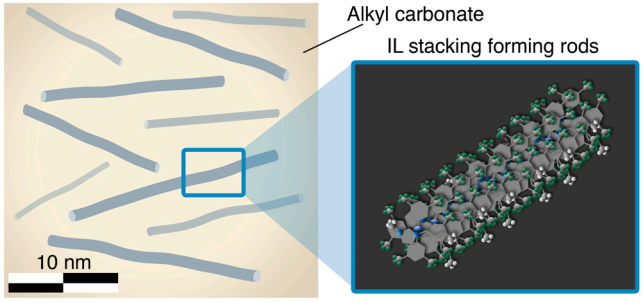

Fig. 3. Structure of the rod-like stacked poly-IL formed by [BMIm][BARF] in alkyl carbonates, as evidenced by SAXS measurements.

However, at these concentrations of [BMIm][BARF], a correlation peak appeared at $q \approx 0.42$–0.45 $Å^{-1}$, which is quite evident in the DMC curves, less pronounced in DEC, and barely recognizable in the DBC samples, suggesting a trend that follows the increasing alkyl chain length and the decreasing dielectric constant of the solvent. Such *q* position translates into a real-space interaction distance of 13–15 Å. A correlation peak accompanied by decreasing forward scattering intensity is representative of repulsive interactions between objects in solution. Since the maximum diameter of the [BMIm][BARF] ion pair is about 20 Å (using the calculated values of 10.9 Å for the anion and 8.6 Å for the stretched cation, estimated with Avogadro software), it is reasonable to assume that the correlation peak might arise from the interactions between undissociated IL pairs in solution, at high [BMIm][BARF] concentration. This effect was, in fact, already observed for other ILs that, even in the absence of a solvent, showed a scattering peak around 0.5 $Å^{-1}$, which was related to the characteristic inverse length scale between polar groups, showing the existence of nano-inhomogeneities in the ionic liquid itself [44]. SAXS results overall are in agreement with the trend already observed by analyzing the Λ/Λ_{NMR} values above, confirming that a large fraction of IL is aggregated in the solutions, especially at lower concentrations. It must be noted that, even if complex nanostructures arising from interactions between ionic liquid molecules with themselves or with other solvents are not uncommon, such worm-like nanostructured inhomogeneities were never observed before. The existence of these peculiar IL domains in organic solvents can be due to the peculiar nature of BARF as the anion. This bulky molecule can assume a rather planar conformation and, instead of establishing H-bonding [33], can be suited to create π-π interactions; all these features can possibly explain the stacking of anions and cations couples, leading to the observed poly-IL conformation.

The FTIR spectra of [BMIm][BARF] in the three solvents were investigated to gain further evidence of the interactions between the different alkyl carbonates and the IL. The FTIR C=O stretching of the alkyl carbonates has a strong and well isolated absorption band in the 1720–1760 cm^{-1} region, which has been used as a probe to investigate the solvation structure and interactions of these solvents with electrolytes [45]. First, we looked into changes in the band's maximum frequency (see Table 5 and Fig. 4A); some red shift of the peak was observed (i.e., to lower wavenumbers) for increasing IL concentration above 50%, and the shift was more intense for DBC (ca. 8-9 cm^{-1} at the highest IL concentration) than for DEC (5-6 cm^{-1}, closer to the spectral resolution), while no significant shift could be detected for DMC. A red shift indicates bond elongation, while a blue shift would indicate bond contraction. Thus, the presence of some red shift for increasing IL concentration already suggests that the electrolyte might interfere with the interactions between alkyl carbonate molecules. The red shift observed in DEC and DBC solutions at 70% is in good agreement with the larger values of Λ/Λ_{NMR} found for the same solutions as compared to the other samples, indicating increased solvation of the IL in charged species.

Alkyl carbonates are known to associate mainly through C—H···O

Table 5
Position (wavenumber) and full width at half maximum (FWHM) of the C=O stretching band of alkyl carbonates in solution with [BMIm][BARF], at different concentrations. DBC = dibutyl carbonate; DEC = diethyl carbonate; DMC = dimethyl carbonate. The error on wavenumbers is ca. ± 0.3 cm^{-1} (lower than the spectral resolution of 4 cm^{-1}), while that on FWHM is ca. ± 1 cm^{-1}.

IL concentration (wt%)	DBC wavenumber (cm^{-1})	DBC FWHM (cm^{-1})	DEC wavenumber (cm^{-1})	DEC FWHM (cm^{-1})	DMC wavenumber (cm^{-1})	DMC FWHM (cm^{-1})
0	1742.4	16	1741.4	17	1749.0	19
5	1742.0	16	1741.5	19	1749.4	21
10	1742.6	17	1741.4	20	1749.2	22
30	1743.1	25	1742.4	26	1751.4	27
50	1744.4	40	1742.3	33	1750.3	30
70	1733.9	38	1735.8	39	1750.2	31

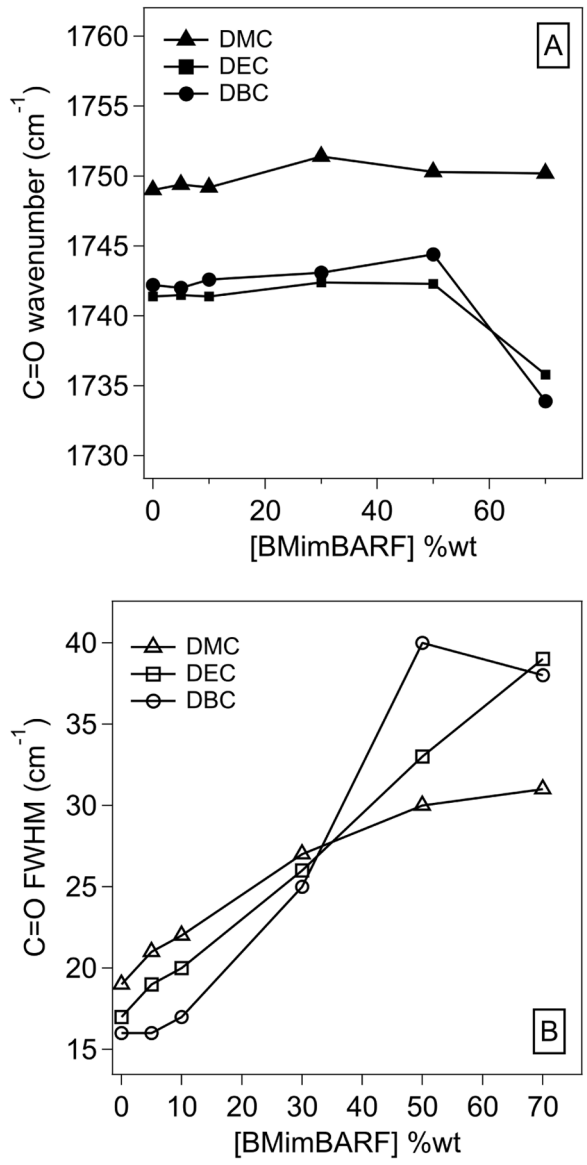

Fig. 4. (A) Position (wavenumber) and B) full width at half maximum (FWHM) of the FTIR C=O stretching band of alkyl carbonates (1720–1760 cm^{-1}), in the presence of [BMIm][BARF] at different concentrations. DBC = dibutyl carbonate; DEC = diethyl carbonate; DMC = dimethyl carbonate.

intermolecular interactions between the carbonyl oxygen of one molecule as proton acceptor and the C—H group of another molecule as proton donor, and such interactions were classified as hydrogen bonds by Wang et al. on the basis of atoms-in-molecules calculations [46]. Instead, according to Finden et al., no H-bonding interactions take place between the imidazolium and the BARF ions, as the bulky trifluoromethyl moieties prevent the anion and cation from coming into close enough proximity for such interactions to occur. [33] It is thus expected that new H-bonding interactions will be established between the alkyl carbonates and the IL, possibly through the carbonate group and the mildly acidic proton in position C2 of the imidazolium cation [47,48].

Indeed, a significant broadening of the C=O stretching band was observed for the different carbonates, and two trends are evident (see Table 5 and Fig. 4B): (i) the band full width at half maximum (FWHM) increased with increasing IL concentration, and (ii) the band broadening at the highest IL concentrations (50–70 wt%) followed the trend DBC ≥ DEC >> DMC. In order to separate the effect of carbonate dilution from that of solvent-IL interaction, the spectra of each IL solution were normalized to the most intense CH stretching absorption of the alkyl carbonates, which is justified considering that solvation strongly affects the stretching and bending modes of C=O and C—O-C groups of the carbonate solvents [49]. However, it must be noticed that the same trends were observed in the spectra even before normalization, which suggests that the effect of solvent-IL interaction is prevalent.

Width increases of the carbonyl band were previously reported by Deepa et al. for PC interacting with lithium imide [50], and by Fulfer et al. for the interaction of linear organic carbonates with lithium hexafluorophosphate [45]. In the first case, it was found that the bandwidths of the well-separated components of the Fermi doublet of the PC C=O stretching band increased with increasing salt concentration in the solvent. In the second case, the authors reported that the frequency distribution of the carbonyl stretch was broadened as the alkyl chain length was increased, likely due to the increased number of possible conformers for carbonate molecules with longer alkyl chains. Therefore, it seems reasonable to hypothesize that also in the case of interactions of alkyl carbonates with [BMIm][BARF], DBC has the most disordered solvation shell, followed by DEC and DMC.

Keeping in mind that [BMIm][BARF] in alkyl carbonates seems to exist prevalently in an aggregate form, as nicely depicted by the analysis of SAXS experiments, if we look at the small fraction of dissociated IL, our combined NMR and FTIR data consistently point to a lower dissociation of [BMIm][BARF] in alkyl carbonates with higher dielectric constants (DMC > DEC > DBC), for higher concentration of IL (> 30–50%). This is also in agreement with SAXS results, as in this concentration range [BMIm][BARF] nanostructured aggregates, observed up to 30% IL, disappear. However, this behavior is opposite to that reported previously for [BMIm][BF_4] and [BMIm][PF_6]: in several studies [37,51] involving a wide range of solvents (water, ethanol, DMSO, acetonitrile and THF), lower dissociation was found for lower dielectric constants. A possible explanation might rely on how the aggregation driving force changes in different BMIm ILs. Because the local structure of nano-sized IL aggregates does not explicitly depend on long-range electrostatic interactions [52], IL units require some mobility to come close and initiate self-assembly. Instead, larger structures of the liquids (i.e., collection of nano-sized aggregates) will be influenced by long-range dipole-dipole interactions [52]. For pairs with less bulky counterions (higher mobility) and strong H-bonding, aggregation is thus

mostly driven by electrostatic forces, and stronger aggregation comes from reduced screening in solvents with lower dielectric constants. This would be in line with the work of Osti et al. [18], who explained the increased ion dissociation of [BMIm][Tf_2N] with increasing solvent polarity by a more efficient screening of the electrostatic interactions, in particular in IL-rich phases. Instead, in the case of bulky and weakly interacting counterions such as BARF, short-range anisotropic van der Waals forces are likely key in the interaction of ionic pairs, and the intrinsic low mobility of the BARF anions might partially hinder their assembly with BMIm; mobility seems to be further reduced in solutions of the IL in alkyl carbonates with increasingly lower dielectric constants (see the trends of anion self-diffusion coefficients, D_-, in Table 2), and possibly less assembly (aggregation) takes place.

4. Conclusion

This work aimed to provide fundamental insight in the multiscale structure and interactions of solutions of the IL [BMIm][BARF] in three alkylcarbonate solvents, i.e., dimethyl, diethyl, and dibutyl carbonate. The estimation of the molar conductivity ratio Λ/Λ_{NMR} showed that the IL was mostly undissociated in these solvents, and SAXS confirmed this by highlighting the presence of rod-like poly(ionic liquid) nanostructures in the 5–30% IL concentration range, formed by the stacking of multiple pairs of anion/cation, which was especially favored in solvents with lower dielectric constant. However, if we look at the small fraction of dissociated [BMIm][BARF] in the samples at higher IL concentration ($>$ 30–50%) some trends emerged as the solvent was changed along the series DMC-DEC-DBC. Our data seem to suggest lower dissociation of the IL in solvents with higher dielectric constants; this is not only evident from the Λ/Λ_{NMR} values, but also trends of the FTIR analysis of the carbonyl stretching bands provide a corroborating picture. This novel finding is surprising, as our results are opposite to those found by previous studies on BMIm ILs with less bulky hydrogen bonding counterions, where increased aggregation was found to occur in solvents with lower dielectric constants. We hypothesize that the nature of the BMIm counterion might play a fundamental role in the assembly of the ions to form nano-sized aggregates. BARF is a weakly coordinating anion with no ability to give strong H-bonding, thus short-range anisotropic van der Waals forces are likely key in the interaction of ionic pairs; in this case, some mobility would be required for close contact between ions, and the slower ions self-diffusion in alkyl carbonates with lower dielectric constants might partially hinder self-assembly into local nanosized structures. In this picture, it is evident that a complex intermix of molecular forces is at play to finely tune the interactions between different species and the resulting nanostructures. When a series of solvents of similar dielectric properties is considered, the otherwise subtle role of dispersion forces and, in the present case, hydrogen bonding vs. van der Waals interactions, can become important enough to reverse the order of solvation capability expected by considering merely the electrostatic component to the interaction potential. This knowledge impacts positively on the understanding of ionic liquid solutions in organic solvents, providing new perspectives in, e.g., electrochemistry, nanoscience and nanotechnology, and potential applications in many fields spanning from batteries, catalysis and extraction, up to bio-applications (antimicrobial and bioengineering).

CRediT authorship contribution statement

Marianna Mamusa: Conceptualization, Methodology, Formal analysis, Writing – original draft, Visualization. **David Chelazzi:** Investigation, Methodology, Formal analysis, Writing – original draft, Writing – review & editing, Visualization. **Michele Baglioni:** Investigation, Formal analysis, Data curation, Writing – original draft, Writing – review & editing. **Sergio Murgia:** Investigation, Methodology, Formal analysis, Writing – review & editing. **Emiliano Fratini:** Conceptualization, Supervision, Funding acquisition, Writing – review & editing. **David Rivillo:** Conceptualization, Supervision, Funding acquisition, Writing – review & editing. **Piet W.N.M. van Leeuwen:** Conceptualization, Supervision, Funding acquisition, Writing – review & editing. **Henri S. Schrekker:** Conceptualization, Supervision, Funding acquisition, Writing – review & editing. **Piero Baglioni:** Conceptualization, Project administration, Funding acquisition, Supervision, Writing – review & editing.

Declaration of Competing Interest

The authors declare that they have no known competing financial interests or personal relationships that could have appeared to influence the work reported in this paper.

Data availability

Data will be made available on request.

Acknowledgments

The European Union Horizon 2020 project APACHE (Active & Intelligent Packaging Materials and Display Cases as a Tool for Preventive Conservation of Cultural Heritage), under the Horizon 2020 Research and Innovation Programme Grant Agreements 814496, is gratefully acknowledged for the financial support. MUR (PRIN 2017249YEF) and CSGI are also acknowledged for funding this work. The Conselho Nacional de Desenvolvimento Científico e Tecnológico - Brasil (CNPq) is acknowledged for financial support. Henri S. Schrekker is grateful to CNPq for the research productivity PQ fellowship. SM gratefully acknowledged Fondazione di Sardegna (FdS Progetti Biennali di Ateneo, annualità 2018).

References

[1] H. Niedermeyer, J.P. Hallett, I.J. Villar-Garcia, P.A. Hunt, T. Welton, Mixtures of ionic liquids, Chem. Soc. Rev. 41 (2012) 7780–7802, https://doi.org/10.1039/c2cs35177c.
[2] S.K. Singh, A.W. Savoy, Ionic liquids synthesis and applications: an overview, J. Mol. Liq. 297 (2020), 112038, https://doi.org/10.1016/j.molliq.2019.112038.
[3] K. Yavir, Ł. Marcinkowski, R. Marcinkowska, J. Namieśnik, A. Kloskowski, Analytical applications and physicochemical properties of ionic liquid-based hybrid materials: a review, Anal Chim. Acta 1054 (2019) 1–16, https://doi.org/10.1016/j.aca.2018.10.061.
[4] R.L. Vekariya, A review of ionic liquids: applications towards catalytic organic transformations, J. Mol. Liq. 227 (2017) 44–60, https://doi.org/10.1016/j.molliq.2016.11.123.
[5] M. Mamusa, M.C. Arroyo, E. Fratini, R. Giorgi, P. Baglioni, Nonaqueous microemulsion in the BmimTf2N/Brij 30/n-Nonane system: structural investigation and application as gold nanoparticle microreactor, Langmuir 34 (2018) 12609–12618, https://doi.org/10.1021/acs.langmuir.8b02420.
[6] P.C. Marr, A.C. Marr, Ionic liquid gel materials: applications in green and sustainable chemistry, Green Chem. 18 (2016) 105–128, https://doi.org/10.1039/C5GC02277K.
[7] M. Mamusa, J. Sirieix-Plénet, R. Perzynski, F. Cousin, E. Dubois, V. Peyre, Concentrated assemblies of magnetic nanoparticles in ionic liquids, Faraday Discuss 181 (2015) 193–209, https://doi.org/10.1039/C5FD00019J.
[8] B.G. Soares, Ionic liquid: a smart approach for developing conducting polymer composites, J. Mol. Liq. 262 (2018) 8–18, https://doi.org/10.1016/j.molliq.2018.04.049.
[9] J. Dupont, On the solid, liquid and solution structural organization of imidazolium ionic liquids, J. Braz. Chem. Soc. 15 (2004) 341–350, https://doi.org/10.1590/S0103-50532004000300002.
[10] H. Xue, R. Verma, J.M. Shreeve, Review of ionic liquids with fluorine-containing anions, J. Fluor. Chem. 127 (2006) 159–176, https://doi.org/10.1016/j.jfluchem.2005.11.007.
[11] M. Dong, K. Zhang, X. Wan, Z. Fang, Y. Hu, Z. Ye, Y. Wang, Z. Li, X. Peng, Enhanced molecular transport in two-dimensional nanoconfined ionic liquids, Appl. Mater. Today 27 (2022), 101458.
[12] J. Wikado, T.J. Huang, T.M. Subrahmanya, H.F.M. Austria, H.L. Chou, W.S. Hung, C.F. Wang, C.C. Hu, K.R. Lee, J.Y. Lai, Bioinspired ionic liquid-graphene based smart membranes with electrical tunable channes for gas separation, Appl. Mater. Today 27 (2022), 101441.

[13] S.I. Wong, H. Lin, J. Sunarso, B.T. Wong, B. Jia, Optimization of ionic-liquid based electrolyte concentration for high-energy density graphene supercapacitors, Appl. Mater. Today 18 (2022), 100522.
[14] M. Kaliner, T. Strassner, Tunable aryl alkyl ionic liquids with weakly coordinating bulky borate anion, Tetrahedron Lett. 57 (2016) 3453–3456, https://doi.org/10.1016/j.tetlet.2016.06.082.
[15] I. Krossing, I. Raabe, Noncoordinating anions—fact or fiction? A survey of likely candidates, Angew. Chem. Int. Ed. 43 (2004) 2066–2090, https://doi.org/10.1002/anie.200300620.
[16] D.R. MacFarlane, N. Tachikawa, M. Forsyth, J.M. Pringle, P.C. Howlett, G. D. Elliott, J.H. Davis, M. Watanabe, P. Simon, C.A. Angell, Energy applications of ionic liquids, Energy Environ. Sci. 7 (2014) 232–250, https://doi.org/10.1039/C3EE42099J.
[17] A.B. McEwen, Nonaqueous electrolytes for electrochemical capacitors: imidazolium cations and inorganic fluorides with organic carbonates, J. Electrochem. Soc. 144 (1997) L84–L86, https://doi.org/10.1149/1.1837561.
[18] N.C. Osti, K.L. Van Aken, M.W. Thompson, F. Tiet, D. Jiang, P.T. Cummings, Y. Gogotsi, E. Mamontov, Solvent polarity governs ion interactions and transport in a solvated room-temperature ionic liquid, J. Phys. Chem. Lett. 8 (2017) 167–171, https://doi.org/10.1021/acs.jpclett.6b02587.
[19] R.A. Di Leo, A.C. Marschilok, K.J. Takeuchi, E.S. Takeuchi, Battery electrolytes based on saturated ring ionic liquids: physical and electrochemical properties, Electrochim. Acta 109 (2013) 27–32, https://doi.org/10.1016/j.electacta.2013.07.041.
[20] K. Gao, X.H. Song, Y. Shi, S.D. Li, Electrochemical performances and interfacial properties of graphite electrodes with ionic liquid and alkyl-carbonate hybrid electrolytes, Electrochim. Acta 114 (2013) 736–744, https://doi.org/10.1016/j.electacta.2013.10.118.
[21] L. Lombardo, S. Brutti, M.A. Navarra, S. Panero, P. Reale, Mixtures of ionic liquid – Alkylcarbonates as electrolytes for safe lithium-ion batteries, J. Power Sources 227 (2013) 8–14, https://doi.org/10.1016/j.jpowsour.2012.11.017.
[22] P.H. Lam, A.T. Tran, D.J. Walczyk, A.M. Miller, L. Yu, Conductivity, viscosity, and thermodynamic properties of propylene carbonate solutions in ionic liquids, J. Mol. Liq. 246 (2017) 215–220, https://doi.org/10.1016/j.molliq.2017.09.070.
[23] P. Tundo, New developments in dimethyl carbonate chemistry, Pure Appl. Chem. 73 (2001) 1117–1124, https://doi.org/10.1351/pac200173071117.
[24] M. Kim, I.J. Kim, S. Yang, S. Kim, Electrochemical properties of organic electrolyte solutions containing 1-ethyl-3-methylimidazolium tetrafluoroborate salt, Res. Chem. Intermed. 41 (2015) 4749–4759, https://doi.org/10.1007/s11164-014-1565-1.
[25] M. Vraneš, N. Zec, A. Tot, S. Papović, S. Dožić, S. Gadžurić, Density, electrical conductivity, viscosity and excess properties of 1-butyl-3-methylimidazolium bis (trifluoromethylsulfonyl)imide+propylene carbonate binary mixtures, J. Chem. Thermodyn. 68 (2014) 98–108, https://doi.org/10.1016/j.jct.2013.08.034.
[26] A. Stoppa, J. Hunger, R. Buchner, Conductivities of binary mixtures of ionic liquids with polar solvents †, J. Chem. Eng. Data 54 (2009) 472–479, https://doi.org/10.1021/je800468h.
[27] A.B. Pereiro, E. Tojo, A. Rodríguez, J. Canosa, J. Tojo, Properties of ionic liquid HMIMPF6 with carbonates, ketones and alkyl acetates, J. Chem. Thermodyn. 38 (2006) 651–661, https://doi.org/10.1016/j.jct.2005.07.020.
[28] K. Fumino, R. ludwing, Analyzing the interaction energies between cation and anion in ionic liquids: the subtle balance between Coulomb forces and hydrogen bonding, J. Mol. Liq. 192 (2014) 94–102.
[29] T. Murphy, R. Hayes, S. Imberti, G.G. Warr, R. Atkin, Ionic liquid nanostructure enables alcohol self-assembly, Phys. Chem. Chem. Phys. 18 (2016) 12797–12809, https://doi.org/10.1039/C6CP01739H.
[30] M. Kawano, K. Sadakane, H. Iwase, M. Matsugami, B.A. Marekha, A. Idrissi, T. Takamuku, Mixing states of imidazolium-based ionic liquid, [C_4mim][TFSI], with cycloethers studied by SANS, IR, and NMR experiments and MD simulations, Phys. Chem. Chem. Phys. 22 (2020) 5332–5346.
[31] J. Dupont, On the solid, liquid and solution structural organization of imidazolium ionic liquids, J. Braz. Chem. Soc. 15 (2004) 341–350.
[32] K. Dong, S. Zhang, J. Wang, Understanding the hydrogen bonds in ionic liquids and their roles in properties and reactions, Chem. Comm. 52 (2016) 6744.
[33] J. Finden, G. Beck, A. Lantz, R. Walsh, M.J. Zaworotko, R.D. Singer, Preparation and characterization of 1-butyl-3-methylimidazolium tetrakis(3,5-bis (trifluoromethyl)phenyl)borate, [bmim]BARF, J. Chem. Crystallogr. 33 (2003) 287–295, https://doi.org/10.1023/A:1023885212233.
[34] W. Levason, D. Pugh, G. Reid, Imidazolium-based ionic liquids with large weakly coordinating anions, New J. Chem. 41 (2017) 1677–1686, https://doi.org/10.1039/C6NJ03674K.
[35] S. Murgia, G. Palazzo, M. Mamusa, S. Lampis, M. Monduzzi, Aerosol-OT forms oil-in-water spherical micelles in the presence of the ionic liquid $BmimBF_4$, J. Phys. Chem. B. 113 (2009) 9216–9225, https://doi.org/10.1021/jp902970n.
[36] S.R. Kline, Reduction and analysis of SANS and USANS data using IGOR Pro, J. Appl. Crstallogr. 39 (2006) 895–900, https://doi.org/10.1107/S0021889806035059.
[37] W. Li, Z. Zhang, J. Zhang, B. Han, B. Wang, M. Hou, Y. Xie, Micropolarity and aggregation behavior in ionic liquid+organic solvent solutions, Fluid Ph. Equilibria. 248 (2006) 211–216, https://doi.org/10.1016/j.fluid.2006.08.013.
[38] H. Tokuda, S. Tsuzuki, M.A.B.H. Susan, K. Hayamizu, M. Watanabe, How ionic are room-temperature ionic liquids? An indicator of the physicochemical properties, J. Phys. Chem. B. 110 (2006) 19593–19600, https://doi.org/10.1021/jp064159v.
[39] R. Naejus, D. Lemordant, R. Coudert, P. Willmann, Excess thermodynamic properties of binary mixtures containing linear or cyclic carbonates as solvents at the temperatures 298.15K and 315.15K, J. Chem. Thermodyn. 29 (1997) 1503–1515, https://doi.org/10.1006/jcht.1997.0260.
[40] L. Mosteiro, E. Mascato, B.E. de Cominges, T.P. Iglesias, J.L. Legido, Density, speed of sound, refractive index and dielectric permittivity of (diethyl carbonate + n - decane) at several temperatures, J. Chem. Thermodyn. 33 (2001) 787–801, https://doi.org/10.1006/jcht.2000.0779.
[41] D. Saar, J. Brauner, H. Farber, S. Petrucci, Ultrasonic and microwave dielectric relaxation of liquid dialkyl carbonates, J. Phys. Chem. 82 (1978) 2531–2535, https://doi.org/10.1021/j100512a014.
[42] O. Russina, A. Sferrazza, R. Caminiti, A. Triolo, Amphiphile meets amphiphile: beyond the polar–apolar dualism in ionic liquid/alcohol mixtures, J. Phys. Chem. Lett. 5 (2014) 1738–1742, https://doi.org/10.1021/jz500743v.
[43] A. Guinier, G. Fournet, C.B. Walker, Small Angle Scattering of X-Rays, J. Wiley&Sons, New York, 1955.
[44] I.A. Sedov, T.I. Magsumov, Highlighting the difference in nanostructure between domain-forming and domainless protic ionic liquids, Phys. Chem. Chem. Phys. 24 (2022) 21477–21494, https://doi.org/10.1039/d2cp02925a.
[45] K.D. Fulfer, D.G. Kuroda, A comparison of the solvation structure and dynamics of the lithium ion in linear organic carbonates with different alkyl chain lengths, Phys. Chem. Chem. Phys. 19 (2017) 25140–25150, https://doi.org/10.1039/C7CP05096H.
[46] Y. Wang, P.B. Balbuena, Associations of Alkyl Carbonates: intermolecular C−H···O Interactions, J. Phys. Chem. A. 105 (2001) 9972–9982, https://doi.org/10.1021/jp0126614.
[47] A. Wulf, K. Fumino, R. Ludwig, Spectroscopic evidence for an enhanced anion–cation interaction from hydrogen bonding in pure imidazolium ionic liquids, Angew. Chem. Int. Ed. 49 (2010) 449–453, https://doi.org/10.1002/anie.200905437.
[48] K. Dong, S. Zhang, D. Wang, X. Yao, Hydrogen Bonds in Imidazolium Ionic Liquids, J. Phys. Chem. A 110 (2006) 9775–9782, https://doi.org/10.1021/jp054054c.
[49] L. Doucey, M. Revault, A. Lautié, A. Chaussé, R. Messina, A study of the Li/Li+ couple in DMC and PC solvents, Electrochim. Acta 44 (1999) 2371–2377, https://doi.org/10.1016/S0013-4686(98)00365-X.
[50] M. Deepa, S.A. Agnihotry, D. Gupta, R. Chandra, Ion-pairing effects and ion–solvent–polymer interactions in $LiN(CF3SO_2)2$–PC–PMMA electrolytes: a FTIR study, Electrochim. Acta 49 (2004) 373–383, https://doi.org/10.1016/j.electacta.2003.08.020.
[51] H.K. Stassen, R. Ludwig, A. Wulf, J. Dupont, Imidazolium salt ion pairs in solution, Chem. Eur. J. 21 (2015) 8324–8335, https://doi.org/10.1002/chem.201500239.
[52] B.S. Jabes, L.D. Site, Nanoscale domains in ionic liquids: a statistical mechanics definition for molecular dynamics studies, J. Chem. Phys. 149 (2018), 184502, https://doi.org/10.1063/1.5054999, 1-9.